

BRITISH GEOLOGICAL SURVEY

Fluid Processes and Waste Management Group

TECHNICAL REPORT WE/99/01

**VLF-R used for
waste-site assessment**

David Beamish

Bibliographic Reference :
Beamish D., 1999.
***VLF-R used for
waste-site assessment.***
*British Geological Survey,
Technical Report, WE/99/01*



British Geological Survey, Keyworth, Nottingham, 1999

©NERC copyright 1999



This report has been generated from a scanned image of the document with any blank pages removed at the scanning stage.
Please be aware that the pagination and scales of diagrams or maps in the resulting report may not appear as in the original

1 Introduction

VLF-R (Resistivity) surveys offer plane-wave but limited bandwidth EM investigations of subsurface resistivity structure. The conventional VLF frequency range (15 to 30 kHz) uses military transmissions at the low frequency end of a set of higher frequency civilian transmissions that can be used to investigate the very near-surface (RadioMT probing of the upper few metres). In contrast to many methods, the techniques use vector (directional) fields to probe 2D and 3D resistivity configurations.

The VLF-R measurement provides a complex surface impedance from the ratio of the induced electric field (E) and orthogonal magnetic field (H). The measurement contains only marginal information on the vertical resistivity distribution since, in effect, only a single frequency is used. The technique has an established mapping capability (Guerin et al., 1994, Beamish, 1998) but can also be used to construct either current density cross-sections (Kaikkonen and Sharma, 1998) or resistivity cross-sections (Beamish, 1994). Increasingly detailed investigations of the near-surface are a requirement of applied geophysical investigations particularly in the environmental and hydrogeological sectors. In order to avoid misleading interpretations, the resolution attributes of single frequency data when combined with recent plane-wave regularised inversion schemes are investigated here.

Being low frequency, VLF fields interact with the near-surface resistivity distribution which lies within their electrical skin/penetration depth (often tens of metres at moderately resistive locations). VLF-R survey data at two former industrial waste sites, aided by wide-band (VLF/RadioMT) synthetic modelling and inversion studies, are used to illustrate their shallow (0 to 20 m) resolution capabilities in conductive environments. The application of 2D regularised (smooth-model) inversion to single-frequency VLF-R survey data is found to be effective provided the noise (non-2D) components of profile data are understood in relation to regularisation and misfit parameters.

2 Background to VLF and RadioMT

The plane-wave, VLF technique conventionally operates in the frequency range from 15 to 30 kHz. The source fields used are line spectra provided by military communication installations (McNeill and Labson, 1991). In moderately resistive environments, the conventional VLF bandwidth provides penetration depths of the order of tens of metres. In principal, the VLF bandwidth can be extended to higher frequencies (i.e. towards 1 MHz) using a variety of civil and commercial radio sources which again have directional propagation characteristics and exist as line spectra. The higher frequencies are intended to provide a much shallower sounding capability since penetration depths can be reduced towards 1 m. One early system, operating at 60 kHz, is described by LaFleche and Jensen (1982). More recently the extension of VLF-R to higher frequencies has been denoted radiomagnetotellurics (RadioMT, Turberg et al., 1994; Zacher et al., 1996). The highest frequencies used in RadioMT are reported to be 240 kHz.

The requirement for multi-frequency observations is a one-dimensional (1D) 'vertical-sounding' concept dating back to the original founding work on magnetotellurics (Cagniard, 1953). For a 1D magnetotelluric resistivity assessment there is a clear requirement to obtain a sufficient density of E/H measurements per decade of bandwidth in the sounding curve in order to adequately resolve subsurface layering. When the resistivity structure is 2D and 3D, subsurface resolution issues are more complicated but clearly depend both on the spectral density content of the observations (including both high and low frequency limits) and the lateral scale and density of the measurements.

In 2D and 3D situations, the detection of the resistivity distribution relies on the excess currents generated at resistivity contrasts (Price, 1973). The distribution of excess currents then modifies the surface fields. In order to provide the excess currents, the fields must have sufficient penetration to interact with the resistivity distribution at any particular depth and location. Figure 2.1 shows the decay of the horizontal E-field amplitude in uniform materials having resistivities from 1 to 500 ohm.m at frequencies of 20 kHz (Fig. 2.1a) and 500 kHz (Figure 2.1b). The horizontal dash line denotes one skin-depth across the set of resistivities. Investigation depths, in a 1D context, can be considered to be a factor of 1.5 times the skin-depths shown (Spies, 1989). For a moderate resistivity of 50 ohm.m, investigation depths range from about 40 m at 20 kHz to about 7.5 m at 500 kHz. When highly conductive materials, such as leachate plumes, are encountered, penetration depths are confined to the upper 10 m at 20 kHz and the upper 2 m at 500 kHz.

As shown above, the VLF bandwidth provides investigation depths that can extend to tens of metres. Conventional VLF data, which are effectively single frequency, are insufficient to resolve 1D (vertical) structure in any detail. At the site investigation scale, however, it is the departures from the background (vertically uniform) structure that are of interest. When single frequency VLF data are collected at a high lateral density (1 to 5 m), the measurements can be used to infer the main elements of the subsurface resistivity distribution. Small-scale, near-surface features (scale-lengths \ll 1 skin depth) will respond galvanically while any larger scale resistivity contrasts may respond inductively depending on their electrical scale lengths at the appropriate frequency (Figure 2.1). The issue of the practical resolution of VLF data at the site investigation scale is explored using a combination of 2D forward/inverse synthetic modelling studies specifically related to two field examples.

3) 2D modelling and inversion

As discussed by Fischer et al. (1983) and Beamish (1994) in order to ensure consistency with a 2-D approach, the directional VLF data must conform to one of the two principal modes of 2-D induction. The assumption of infinite strike (which defines the 2-D case) provides two decoupled modes involving separate combinations of the field components. The TE-mode (or E-polarisation, electric field parallel to strike) involves surface fields of E_x , H_y and H_z . The TM-mode (or H-polarisation, magnetic field parallel to strike) involves the surface fields H_x , E_y and E_z . Due to the directional nature of VLF

measurements, we require therefore that the measurements be made in, at least one, of the two principal directions. Where the geological strike is not known, the survey option of taking measurements from several azimuthally-distinct transmitters is suggested.

The TE-mode provides VLF-R and VLF-Z data and anomaly wavelengths are generally larger than their TM-mode counterparts. In the TM-Mode, no VLF-Z field is generated and thus combined measurements of VLF-R and VLF-Z can be used as a means of mode identification. The two case studies provide examples of individual mode modelling and inversion. Joint mode inversion is also possible (Beamish, 1994) but is not considered here.

The starting point in the modelling of VLF data are the developments in non-linear inversion which have arisen in the context of the multi-frequency MT technique. The new approaches involve regularising an otherwise 'ill-posed' problem by introducing a smooth or minimum-structure constraint. In 2-D inversion, the problem of equivalence becomes particularly acute because of the larger number of degrees of freedom within the model space. The essential point is that the minimum-structure inversion concept acknowledges this fact and allows the construction of credible (non-extreme) resistivity models.

For 2-D MT inversion, deGroot-Hedlin and Constable (1990) implemented a minimum-structure inversion which is referred to as OCCAM and is based on the finite-element forward solution of Wannamaker et al. (1987). A more rapid 2D inversion code involving a non-linear, conjugate gradient (NLCG) algorithm has recently been described by Rodi and Mackie (1998). The algorithm implements first-derivative smoothing and includes a regularisation parameter (τ) that controls the degree of model smoothness/roughness (often a trade-off with misfit). VLF studies using the former method were described by Beamish (1994). The latter method is used in the present study since it readily permits the use of a regular subsurface finite-difference grid comprising in excess of 100x100 1 m cells.

The measured data should possess error bounds. An *exact* fit between measured and modelled data is rarely warranted. The error bound must comprise the variance associated with physical measurement but it can also encompass the degree to which a particular level of modelling (e.g. 1D, 2D or 3D) is thought to be appropriate. Given a set of N observations (o_i , $i=1,N$) with standard errors (σ_i), the concept is to only fit the observations to within a prescribed level of misfit. When the data and errors conform to Gaussian behaviour the chi-square (χ^2) statistic is a natural measure of misfit :

$$\chi^2 = \sum (o_i - m_i)^2 / \sigma_i^2$$

where m_i refers to the i 'th model response. An r.m.s. measure of misfit defined as χ^2/N with an expectation value of unity is used here.

4) Modelling and inversion : synthetic data

Two type models have been investigated each of which allows resolution issues of the field data examples to be examined. Both models comprise a typical site-investigation profile length of 100 m. The central subsurface comprises 100x100, 1 m cells before expansion to satisfy boundary condition requirements. The two models are shown in Figure 4.1. Model 1, shown in Figure 5.1a, is a representation of a concealed, near-surface, conductive waste-pit with near-surface resistive features. The conducting pit also contains a further small zone (2x2 m) of highly conducting (0.1 ohm.m) material. Model 2 shown in Figure 5.1b contains two small-scale conductive features located at depths between 5 and 15 m. Near-surface resistive features are also present. In both models the background host material has a resistivity of 50 ohm.m and thus both conductive and resistive targets are present.

In order to examine the context of single frequency VLF observations, the response at a range of higher frequencies (RadioMT) has been examined. Four frequencies of 20 kHz (VLF), 50 kHz, 200 kHz and 500 kHz are used. The range of electrical scale lengths for the problem is large and skin-depths are shown in Table 1. The skin-depths range from 25 m at 20 kHz to 5 m at 500 kHz in the host background of 50 ohm.m.

Table 1. Skin-depths in metres for VLF and RadioMT frequencies (20 to 500 kHz) for uniform materials having resistivities from 0.1 to 1000 ohm.m.

Resistivity ohm.m	20 kHz	50 kHz	200 kHz	500 kHz
0.1	1.12	0.71	0.36	0.22
1	3.56	2.25	1.12	0.71
50	25.1	15.9	7.95	5.03
200	50.3	31.8	15.9	10.1
500	79.5	50.3	25.15	15.9
1000	112.5	71.1	35.57	22.5

4.1) Model 1

The VLF-R TE-mode response of Model 1 at four frequencies is shown in Figure 4.2. All four response characteristics follow a similar pattern with the main perturbation caused by the largest scale feature (the conducting pit from 20 to 60 m). At the lowest (VLF) frequency, the response fails to return to the half-space values of 50 ohm.m and 45 degrees. Changes in spatial gradient, due to the near-surface resistive features are more apparent with increasing frequency.

The response characteristics of all four frequencies contain diagnostic information on the subsurface resistivity distribution. The degree of reliable information is examined by inverting the TE-mode data first using all four frequencies and then by inverting only the lowest (VLF) frequency data. The inversions of the synthetic data use apparent resistivity

and phase data sampled at 1 m intervals. Nominal 2 % errors have been assigned to the data and no random errors have been introduced. The analysis undertaken therefore represents the best possible resolution case. An initial half-space of 100 ohm.m was used to initiate the inversions. Using the assigned error limits, an rms misfit of unity is achieved by both inversions. Since the data are ideal, all features of the data (Fig. 4.2) can be accurately reproduced.

The TE-mode inversion results are shown in Figure 4.3 for both the single frequency analysis (Fig. 4.3a) and the four frequency analysis (Fig. 4.3b). The outline of the original model is shown by the heavy broken lines. Inversion models with smooth constraints cannot recover discontinuous resistivity distributions; they are imaged by gradients. The main resistivity element recovered by the single frequency analysis is the conductive pit. The upper surface of the concealed feature is a much better resolved feature than the base; the decreasing resolution with depth is a general attribute. The sloping edge of the pit is only marginally detected and the highly conducting interior zone is undetected. The two at-surface, shallow resistive zones are largely unresolved.

In the TE-mode, a much higher level of resolution of all the original model features is achieved using four frequencies (Fig. 4.3b). The gradients of the smooth model outline both conductive and resistive features of the model. The small-scale conductive zone, within a conductive zone, is resolved and the western sloping edge of the conducting pit is indicated by the attitude of the gradients. Again the worst resolved feature of the analysis is the base of the conducting pit and its true depth must be inferred

For comparison purposes, the TM-mode response of Model 1 is shown in Figure 4.4. The TM-mode produces a discontinuous electric field at lateral boundaries and, as a consequence, large and rapid response characteristics are generated. The spatial wavelengths produced by the TM-mode are much smaller than their TE-mode counterparts and the amplitude perturbations are much larger.

4.2) Model 2

The VLF-R TM-mode response of Model 2 at four frequencies is shown in Figure 4.5. It should be noted that the spatial wavelengths produced by the TM-mode are much smaller than their TE-mode counterparts. All four response characteristics follow a similar pattern with the main perturbations caused by anomalies between 40 and 80 m. The increase in apparent resistivities from the host value of 50 ohm.m is deceptive.

Again the analysis is undertaken by inverting the TM-mode data first using all four frequencies and then by inverting only the lowest (VLF) frequency data. The inversions used apparent resistivity and phase data sampled at 1 m intervals. Other details are as used previously for Model 1.

The TM-mode analysis models produced are shown in Figure 4.6 for the single frequency analysis (Fig. 4.6a) and for the four frequency analysis (Fig. 4.6b). The outline of the

original model is shown by the heavy broken lines. In the single frequency (20 kHz) model there are indications of all three structural elements of the original model (both resistive and conductive). The at-surface resistive zone, including the edge 'step' is resolved. The central conducting zone at a depth of 5 m is imaged with a shape distortion due to the (unresolvable) extended base. The second small conducting zone is indicated but the imaged resistivity is too high.

When four frequencies are used (Fig. 4.6b) tighter spatial gradients resolve the features of the model with greater resolution and resistivity values are more precise. The gradients of the smooth model outline both conductive and resistive features of the model. The 2 m thick extension to the central conductive zone is unresolvable and produces an elongate feature rather than a true L shape. The second small conducting zone is again imaged but with a resistivity value that is too high.

5) Modelling and inversion : field data

The two single-frequency field examples both come from assessments of sites which have been used for the disposal of industrial wastes. The first example comes from a waste disposal pit containing tars and tar-derived leachates. The tar is intrinsically acidic and conductive ($< 15 \text{ ohm.m}$) compared to the host mudrock ($> 50 \text{ ohm.m}$). Shallow ($< 2 \text{ m}$) backfill used largely iron-rich furnace slag. The second example uses data obtained across a former quarry in sandstone which was used for a wide-variety of industrial wastes with existing products being lime slurries, brines, metal waste, DNAPL's and acidic leachates. In both cases the measurements were made with a Scintrex IGS-2 system employing 5 m dipoles and capacitive electrodes. The two examples both use the Rugby (UK) VLF transmitter (GBR, 16 kHz).

5.1) Example 1

This example uses a 100 m profile of observations made in the TE-mode with a station sampling of 5 m. The example relates to the previous resolution assessments of synthetic model 1. The data obtained are shown by the symbols in Figure 5.1. The main elements of the observed data are similar to those presented in Figure 3.1. The data have been inverted using the NLCG method. The subsurface comprises a 100 x 100, 1 m grid across the central region. The inversions were initiated using a half-space of 25 ohm.m. As with the synthetic data, arbitrary error bounds of 2% were assigned for the analysis of misfit.

Figure 5.2 shows the results of two inversions. In Figure 5.2a, a smoothing parameter of $\tau=30$ was used and the rms misfit achieved was 5%. The fit of the model to the data is shown in Figure 5.1 by the continuous solid line. It can be seen that while moderate wavenumber components of the data are well modelled, certain high wavenumber components generate the greatest level of misfit. Some of the largest misfits arise at the data sampling scale of 5 m. The resulting inversion model (Figure 5.2a) contains largely moderate wavenumber components in the resistivity distribution.

It is possible to reduce the misfit by decreasing the degree of smoothing in the inversion model. Figure 5.2b shows the result of decreasing the smoothing parameter ($\tau=1$) which allows the rms misfit to decrease from 5% (Figure 5.2a) to 4%. The fit of this second model to the data is shown in Figure 5.1 by the broken line. It is evident that only a marginal improvement in fit is achieved. The resulting model however, while retaining the moderate wavenumber features of the previous model, amplifies a series of high wavenumber components of the resistivity distribution. It is likely that only the resistivity distribution shown in Figure 5.2a is warranted by the fit to the data (with measurement errors of 1 ohm.m in apparent resistivity and 1 degree in phase). The high wavenumber components in the measurements are likely to be the result of small-scale (< E-field measurement scale length) irregularities in the near-surface. These features present the profile measurements with a three dimensional and multi-mode response which cannot be modelled by 2D (or 3D) procedures. The resulting noise components are well described as 'debris noise'.

The result of Figure 5.2a represents the minimum structural model that is consistent with the observations. Discontinuous features, if they exist, are represented by the changes in gradients. The synthetic modelling of Figure 3.2 can be used as a guide in the interpretation of the field inversion result. The main conducting tar pit exists between 20 and 60 m and is concealed by 2 to 3 m of more resistive backfill. The margins of the pit (in terms of bulk resistivity) slope inwards and a main conducting phase (< 1 ohm.m) is detected at depths between 5 and 10 m at profile distances of 25 to 30 m. A reasonable estimate of the depth of the pit is 12.5 m.

5.2) Example 2

The second example uses a profile of 83 observations made in the TM-mode with a station sampling of 1 m. The example relates to the previous resolution assessments of synthetic model 2. The 1 m data interval represents oversampling since the dipole length remains fixed at 5 m. The discontinuous nature of the TM-mode response and the likely presence of debris noise suggests that oversampling may be appropriate in the absence of an ability to use dipole lengths of 1 m.

The data obtained are shown by the symbols in Figure 5.3. Only crude similarities between the observed data and those of the synthetic model (Figure 4.5) are evident. In this example, apparent resistivities reach a lower instrument level of 1 ohm.m and phase values reach a value of 90 degrees. The data have been inverted using the NLCG method with modelling details as for the former example.

Figure 5.4 shows the results of two inversions. In Figure 5.4a, a smoothing parameter of $T=30$ was used and the rms misfit achieved was 5%. The fit of the model to the data is shown in Figure 5.3 by the continuous solid line. It can be seen that the misfit largely stems from the observed phase excursions to high values. The resulting inversion model (Figure 5.4a) contains largely moderate wavenumber components in the resistivity distribution.

It is possible to reduce the misfit by decreasing the degree of smoothing in the inversion model. Figure 5.4b shows the result of decreasing the smoothing parameter ($T=1$) which allows the rms misfit to decrease from 5% to 3.6%. The fit of this second model to the data is shown in Figure 5.3 by the broken line. It is evident that only a marginal improvement in fit is achieved. The resulting model however, while retaining the moderate wavenumber features of the previous model, amplifies two high wavenumber components of the resistivity distribution which are associated with the maximum phase excursions. It is likely that only the resistivity distribution shown in Figure 5.4a is warranted by the fit to the data. The high wavenumber components introduced into the most conductive zones are likely to be 3D effects which cannot be effectively modelled.

The result of Figure 5.4a represents the minimum structural model that is consistent with the observations. Discontinuous features, if they exist, are represented by the changes in gradients. The synthetic data inversion result of Figure 4.6a can be used as a guide in the interpretation of the field inversion result. A large wavenumber trend of low resistivity values (< 10 ohm.m) suggests a dip of conducting infill from west to east across the western margin of the profile. Several metres of resistive infill occur between 50 and 100 m. Two highly conducting (< 1 ohm.m) zones are detected between depths of 5 and 10 m, centred on profile locations of 70 and 90 m. The zones are laterally compact and may be less than 5 m in width. The base of conducting infill of the quarry (the original quarry floor is thought to be at a depth of 25 m) cannot be resolved due to rapid attenuation in the conductive environment.

6) Summary and conclusions

The aim of this study has been to demonstrate the utility of single frequency VLF-R data in the investigation of near-surface environmental problems. It has been noted that VLF frequencies provide the deepest penetrations of the multi-frequency extended method of RadioMT. The modelling study has considered both applications. Conventional VLF data, which are effectively single frequency, are insufficient to resolve 1D (vertical) structure in any detail. At the site investigation scale, however, it is the departures from the background (vertically uniform) structure that are of interest.

The synthetic modelling and inversion examples demonstrate the extent to which single frequency VLF data possess a lower resolution than their multi-frequency, RadioMT counterparts. In the examples shown, the RadioMT resolution analysis used VLF data (20 kHz) and a further 3 sets of response data. The additional constraints essentially provide only second-order improvements in the detection of target structure boundaries. It appears that the spatial gradients generated at the lowest (VLF) frequency contain a high degree of information on the configuration of the subsurface resistivity distribution.

The data in the synthetic model studies contain no noise and are therefore an idealised case. They demonstrate that the highest possible lateral measurement scale should be used, particularly for studies involving the discontinuous TM-mode response. In cases where the instrument and/or signal/noise issues preclude E-field dipole lengths of < 5 m,

it is still useful to perform measurements at a 1 m interval. Typically, the noise present in VLF surveys at the site investigation scale is not measurement noise at the instrumental level. Since vector (directional) fields are employed, departures from a single-mode, 2D response are likely. When the noise is caused by small-scale (\ll E-field dipole scale length) irregularities, inversion models close to the minimum misfit may be inappropriate.

7) References

- Beamish, D., 1994. Two-dimensional, regularised inversion of VLF data. *Journal of Applied Geophysics*, 32, 357-374.
- Beamish, D., 1998. Three-dimensional modelling of VLF data. *J. Applied Geophysics*, 39, 63-76.
- Cagniard, L., 1953. Basic theory of the magneto-telluric method of geophysical prospecting. *Geophysics*, 18, 605-635.
- Constable, S.C., Parker, R.L. and Constable, C.G., 1987. Occam's inversion : a practical algorithm for generating smooth models from EM sounding data. *Geophysics*, 92: 289-300.
- deGroot-Hedlin, C.M. and Constable, S.C., 1990. Occam's inversion to generate smooth, two-dimensional models from magnetotelluric data. *Geophysics*, 55: 1613-1624.
- Fischer, G., Le Quang, B.V. and Muller, I., 1983. VLF ground surveys, a powerful tool for the study of shallow two-dimensional structures. *Geophys. Prosp.*, 31: 977-991.
- Guerin, R., Tabbagh, A., Benderitter, Y. and Andrieux, P., 1994. Invariants for correcting field polarisation effects in MT-VLF resistivity mapping. *J. Applied Geophysics*, 32: 375-383.
- Kaikkonen, P. and Sharma, S.P., 1998. 2-D nonlinear joint inversion of VLF and VLF-R data using simulated annealing. *J. Applied Geophysics*, 39, 155-176.
- LaFleche, P.T. and Jensen, O.G., 1982. Wave impedance measurements at 60 kHz. In : L.S. Collett and O.G. Jensen (Editors), *Geophysical Applications of Surface Wave Impedance Measurements*, Geological Survey of Canada, Paper 81-15, pp. 67-78.
- McNeill, J.D. and Labson, V.F., 1991. Geological mapping using VLF radio fields. In: Nabighian, M. (Editor), *Electromagnetic Methods in Applied Geophysics, Part B: Application*. SEG, Tulsa, pp. 521-640.

Price, A.T., 1973. The theory of geomagnetic induction. *Phys. Earth Planet. Int.*, 7, 227-233.

Rodi, W. and Mackie, R.L., 1998. Nonlinear conjugate gradients algorithm for 2-D magnetotelluric inversion, *Geophysics*, submitted.

Spies, B.R., 1989. Depth of investigation in electromagnetic sounding methods. *Geophysics*, 54: 872-888.

Tabbagh, A., Benderitter, Y., Andrieux, P., Decriaud, J.P. and Guerin, R., 1991. VLF resistivity mapping and verticalization of the electric field. *Geophys. Prosp.*, 39: 1083-1097.

Turberg, P., Muller, I. And Flury, F., 1994. Hydrogeological investigations of porous environments by radiomagnetotelluric-resistivity. *J. Appl. Geophysics*, 31: 133-143.

Wannamaker, P.E., Stodt, J.A. and Rijo, L., 1987. A stable finite element solution for two-dimensional magnetotelluric modelling. *Geophys. J. R. astr. Soc.*, 88: 277-296.

Zacher, G., Tezkan, B., Neubauer, F.M., Hordt, A. And Muller, I., 1996. Radiomagnetotellurics: a powerful tool for waste-site exploration. *European J. Environ. And Engineering Geophysics*, 1: 139-159.

Fig. 2.1

Decay of E-field amplitude in homogenous materials

Horizontal dotted line denotes skin-depth i.e. point at which the primary field has decayed to 1/e of the surface value

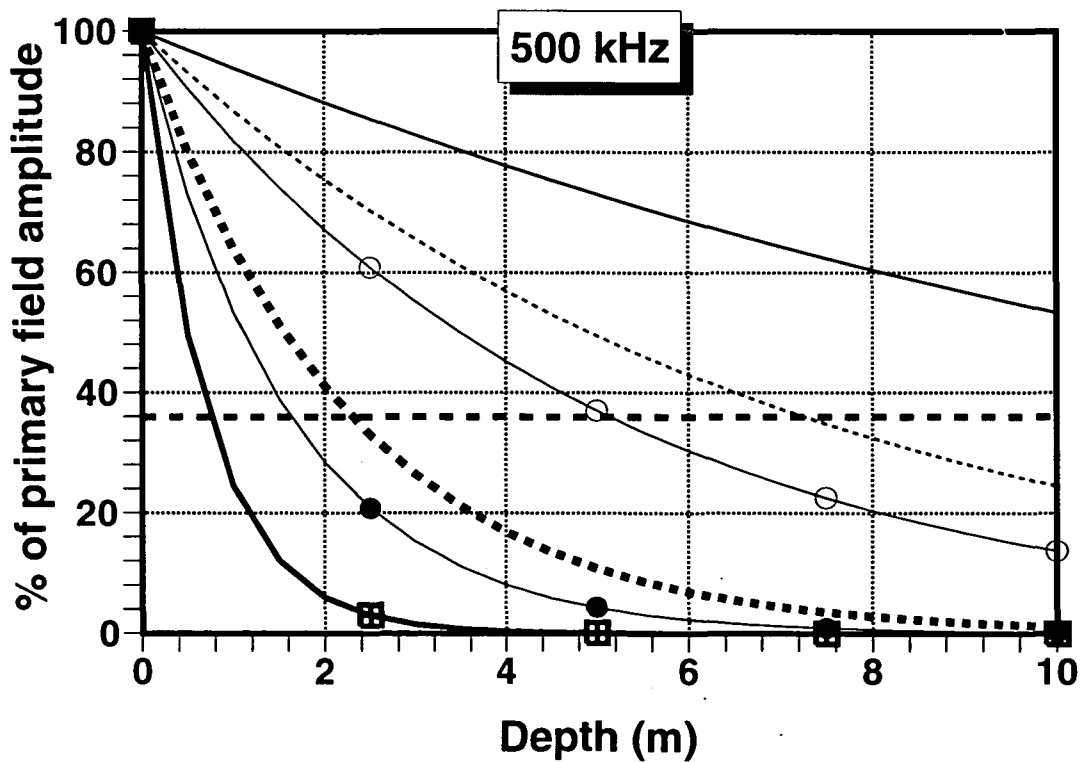
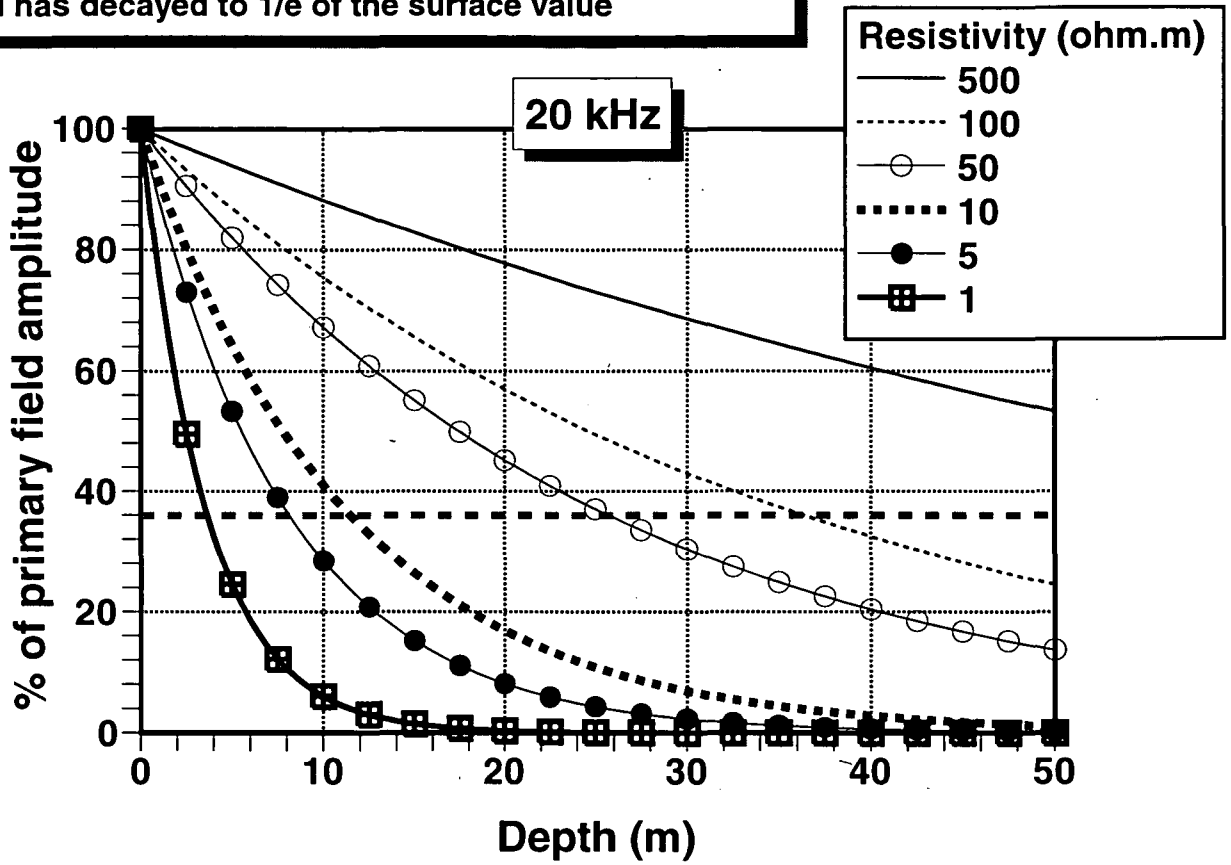
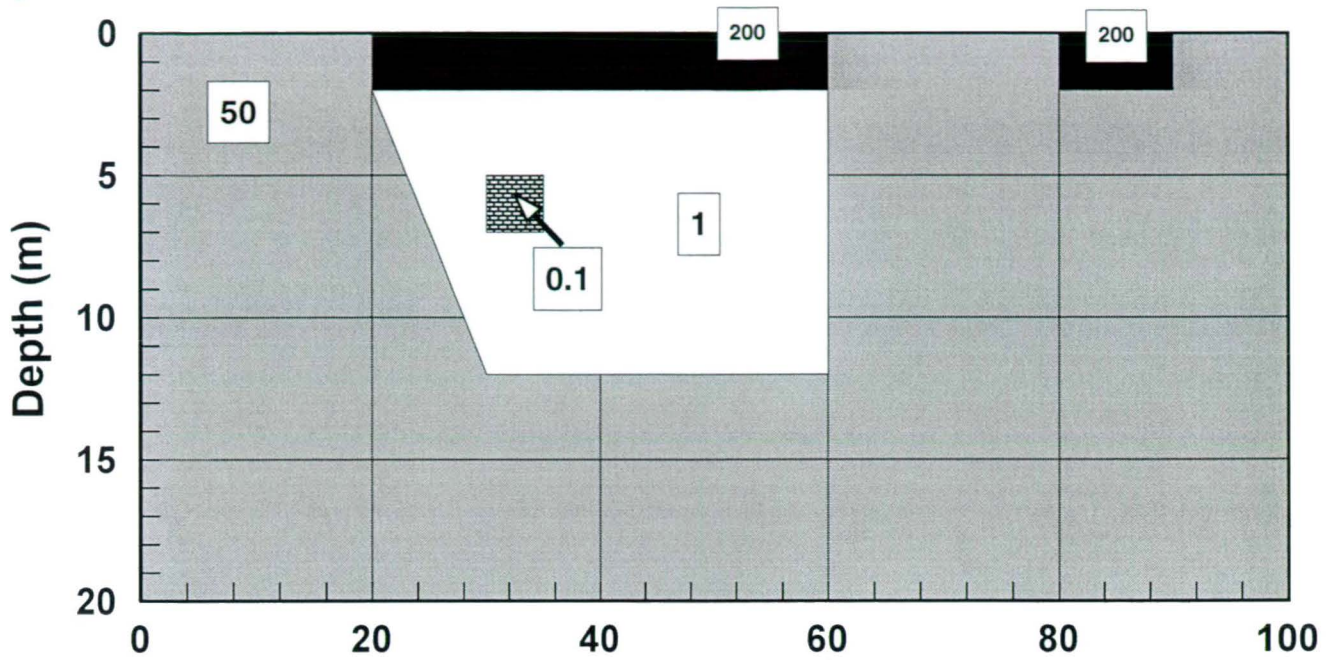
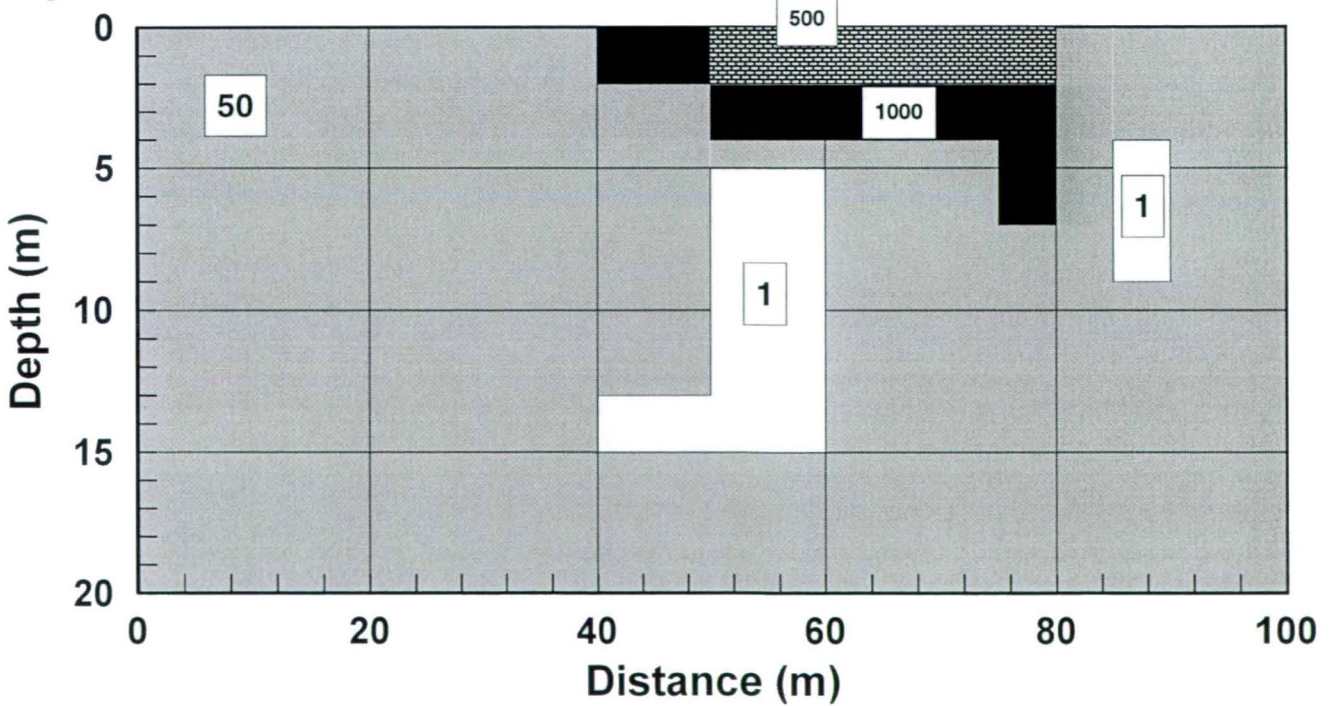


Fig. 4.1

a) Model 1



b) Model 2



Resistivity values are shown in boxes

Fig. 4.2

Model 1 TE-mode

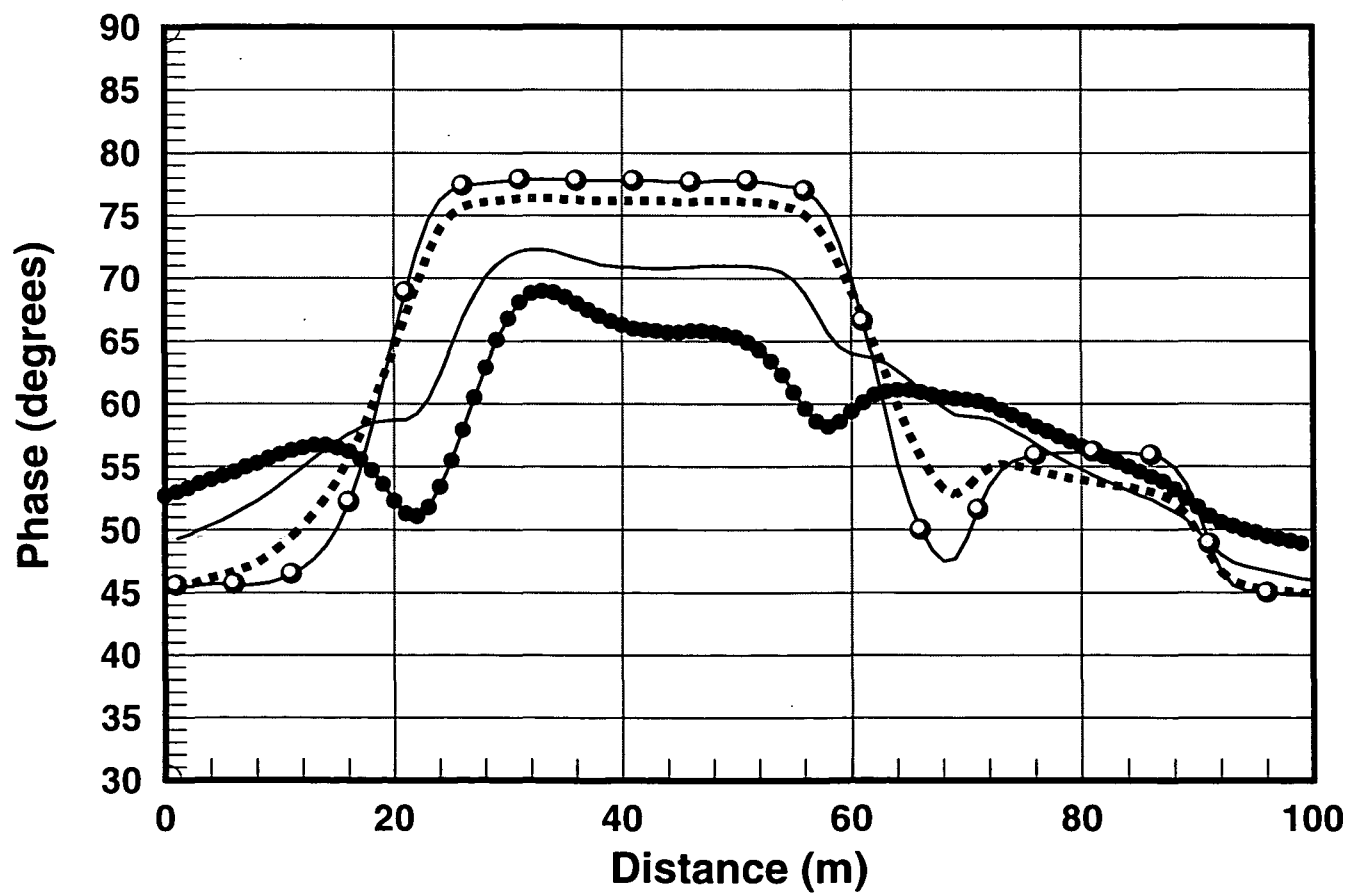
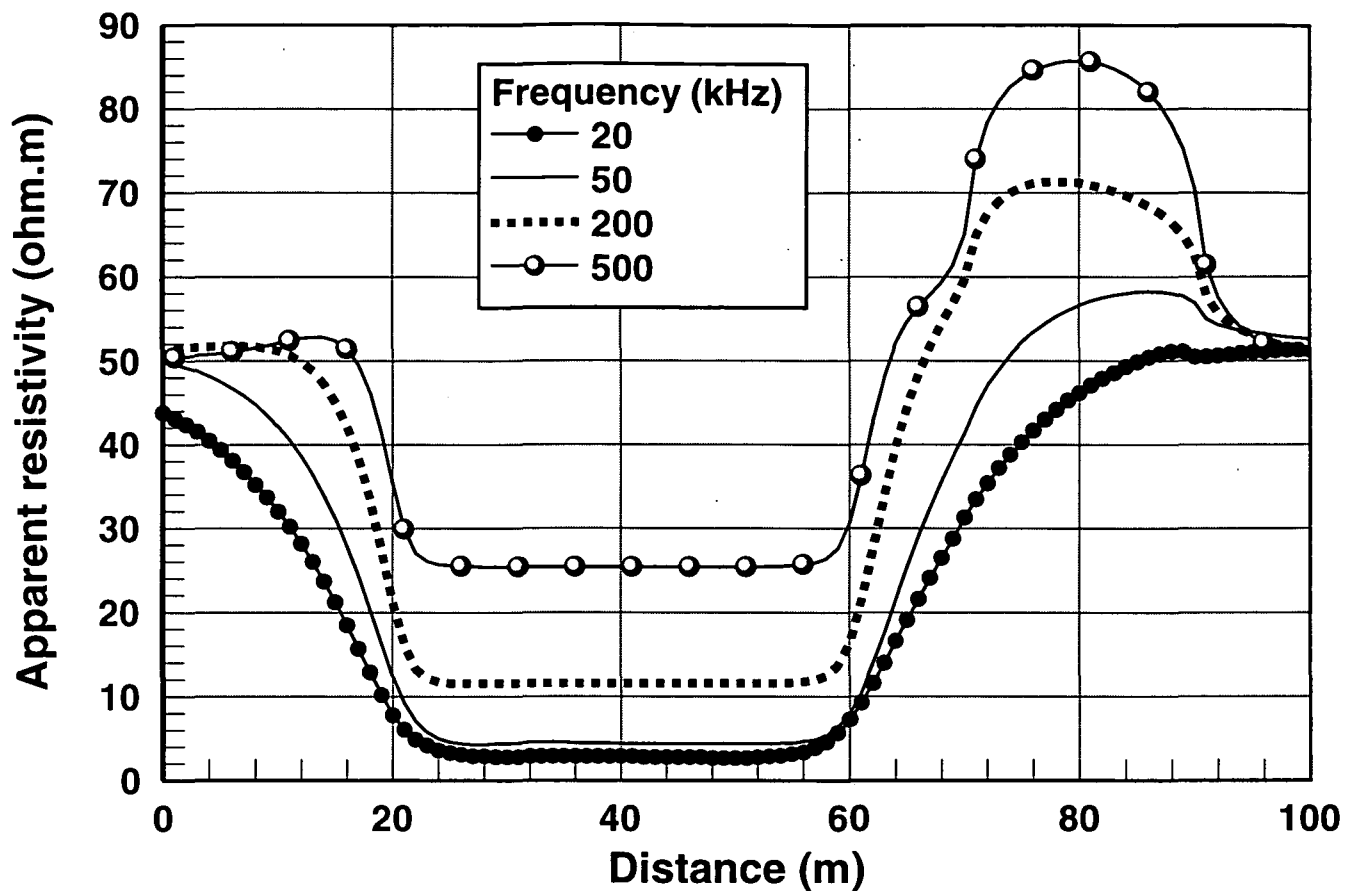
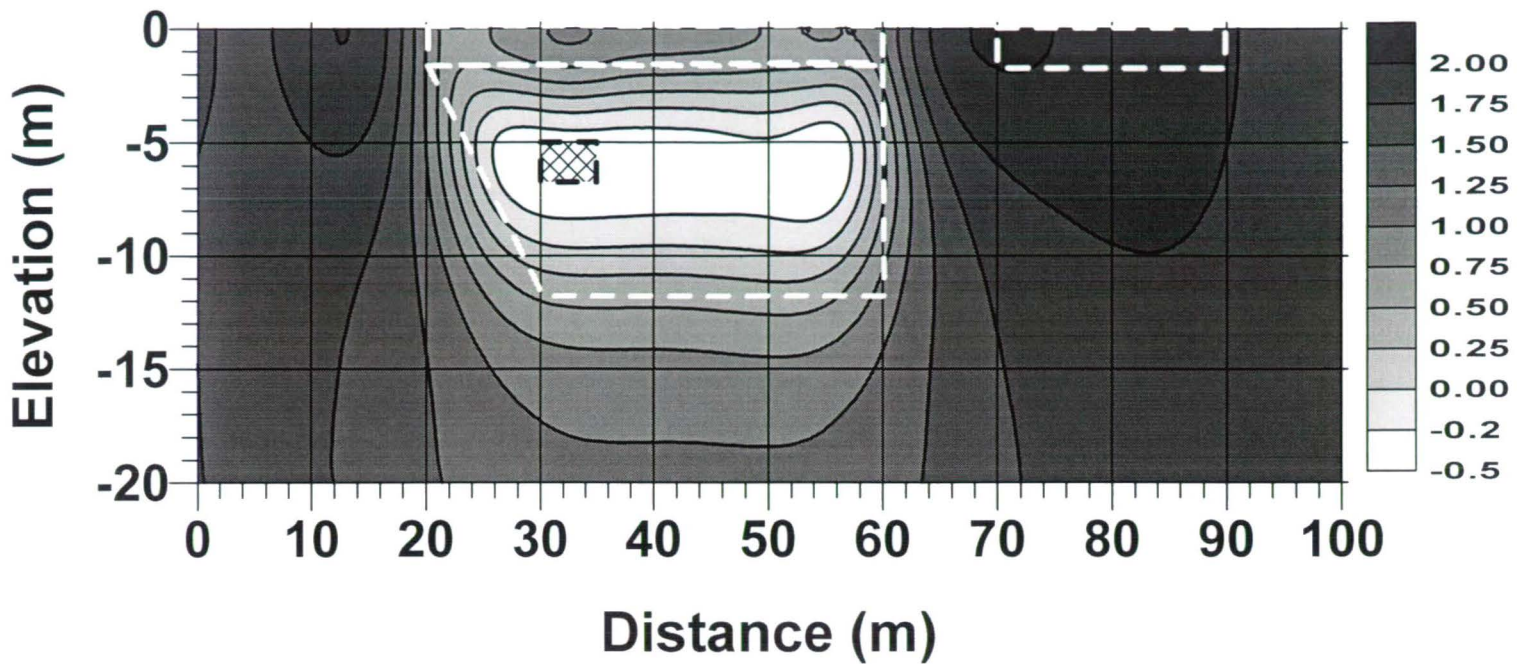


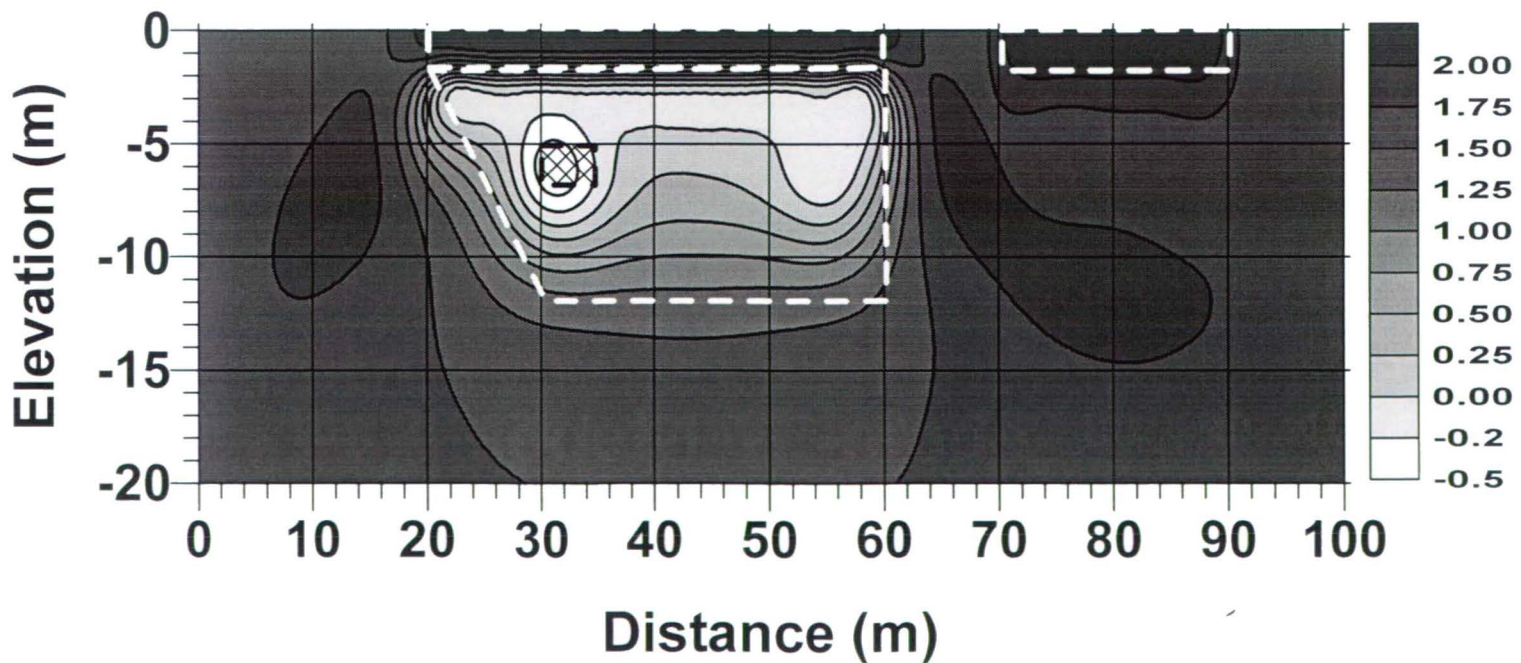
Fig. 4.3

Model 1 TE-mode

a) 1 Frequency



b) 4 Frequencies



Cross-section contoured using the logarithm of resistivity. Scale bar in log (resistivity ohm.m)

Fig. 4.4

Model 1 TM-mode

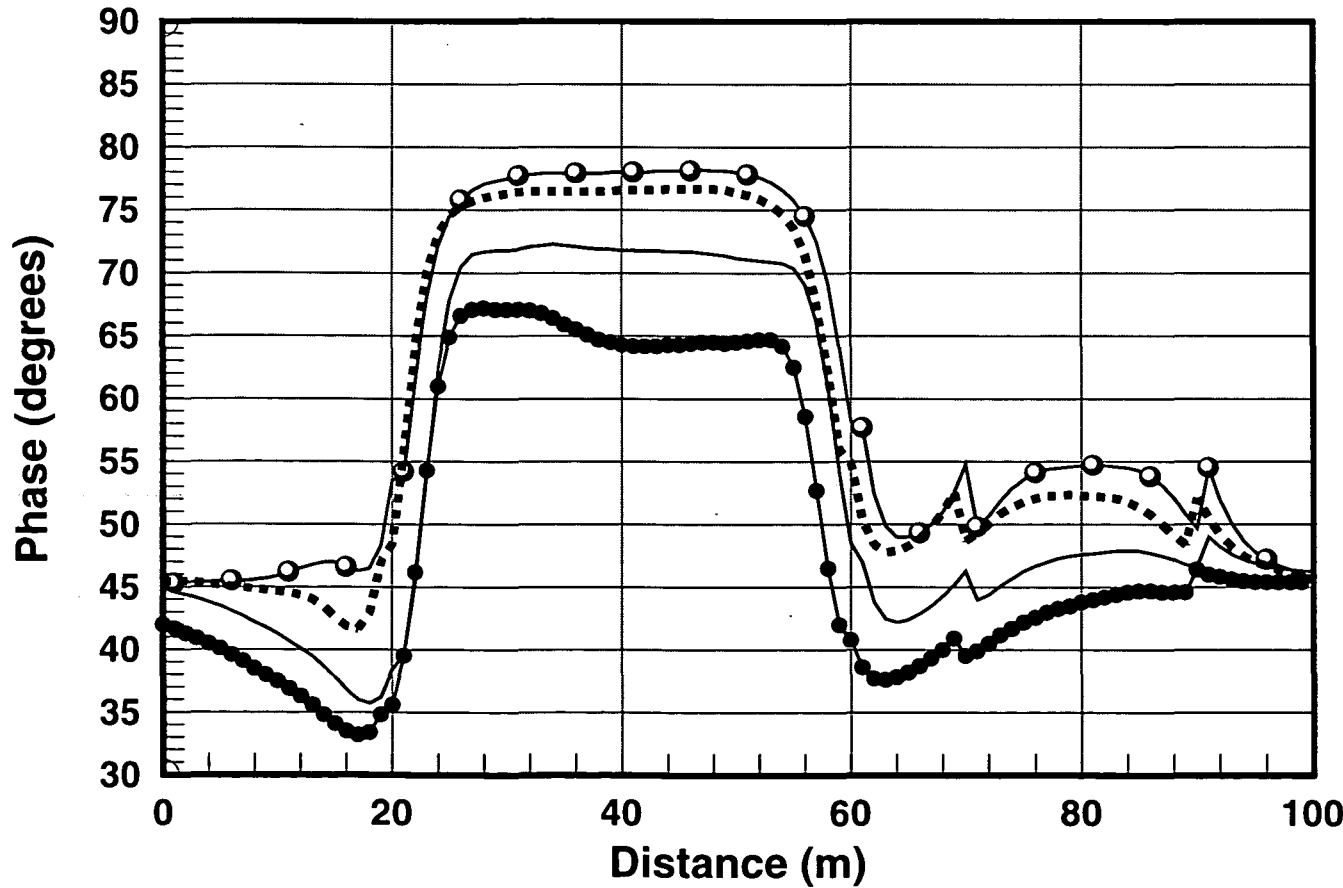
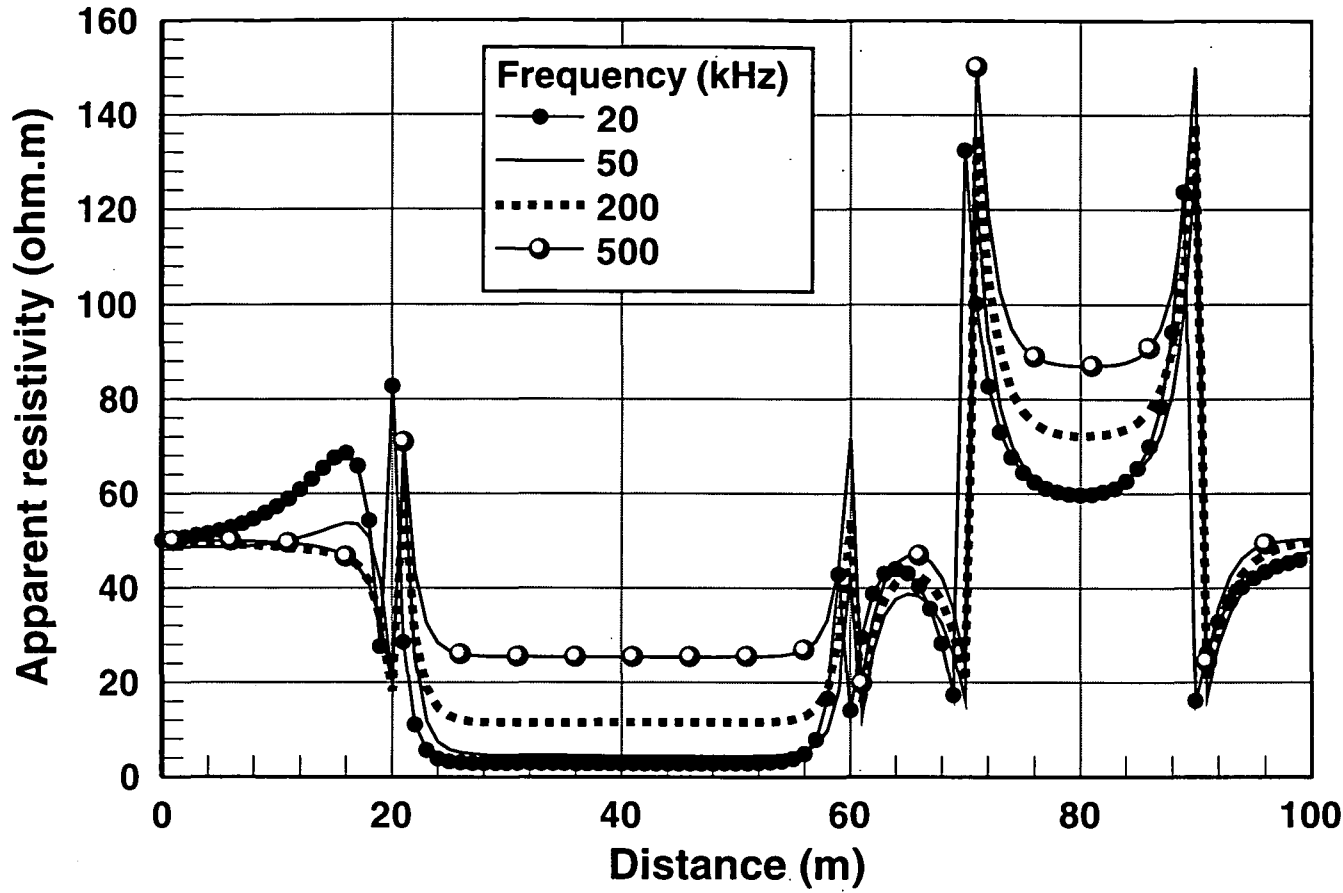


Fig. 4.5

Model 2 TM-mode

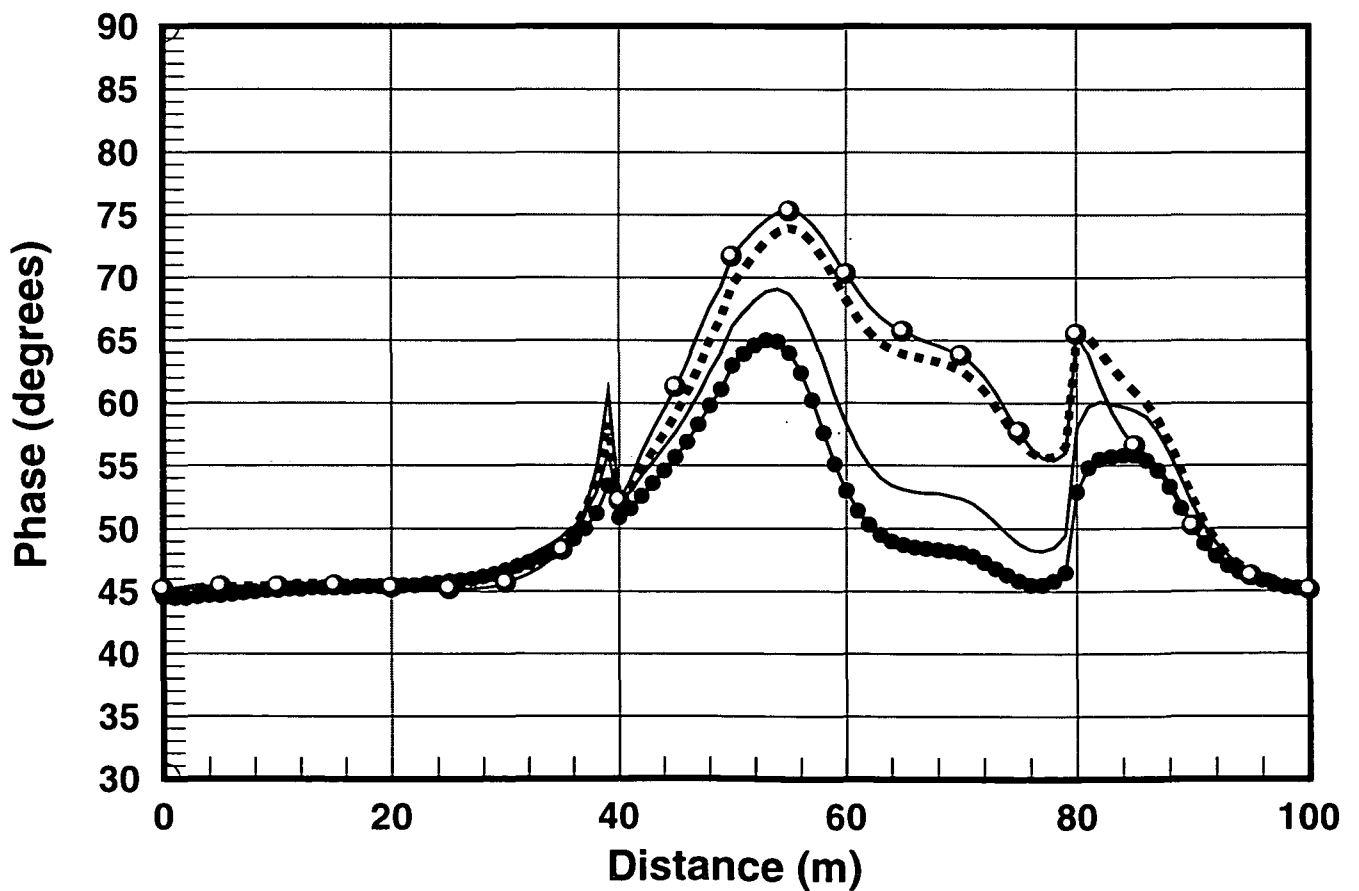
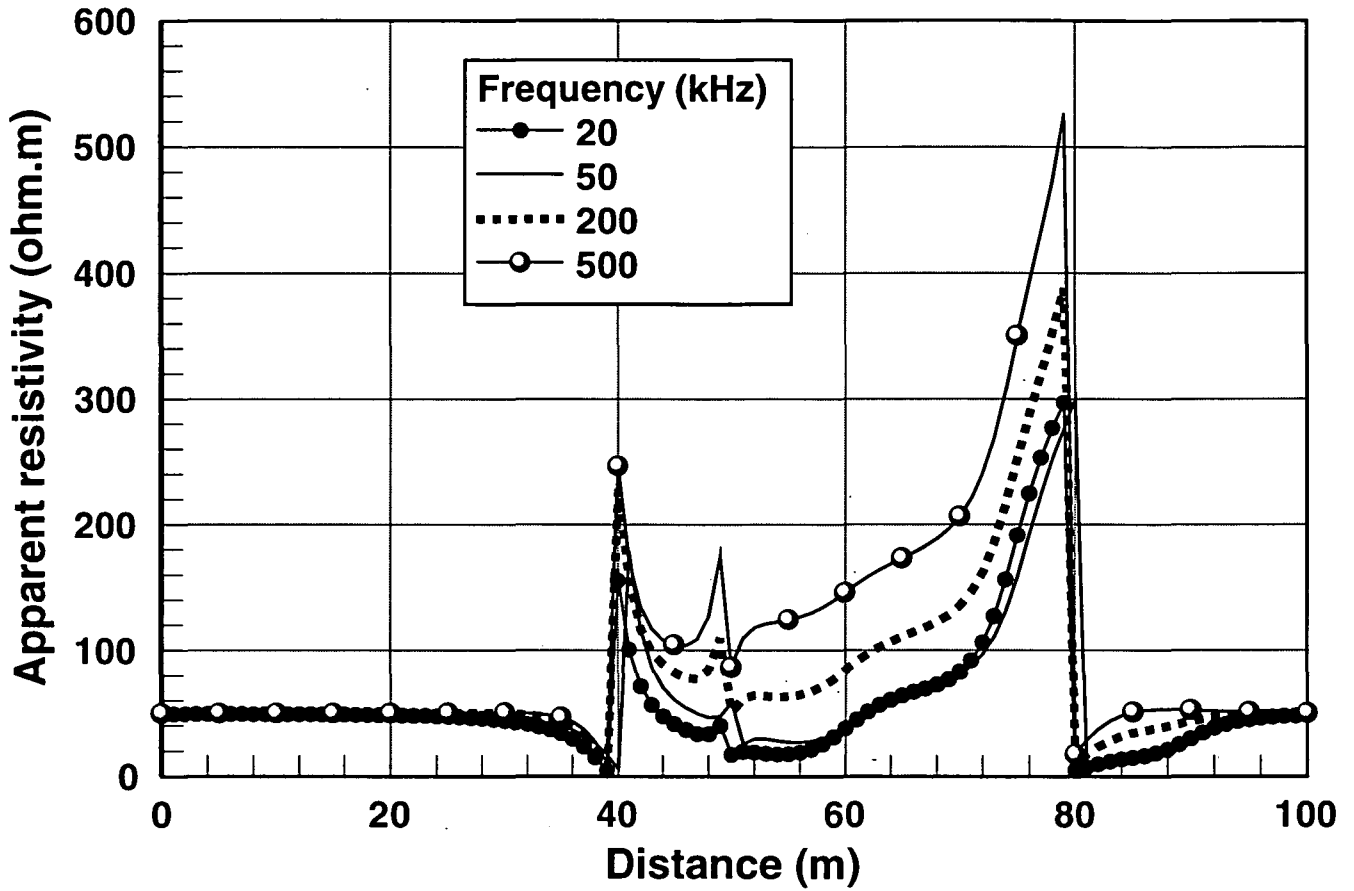
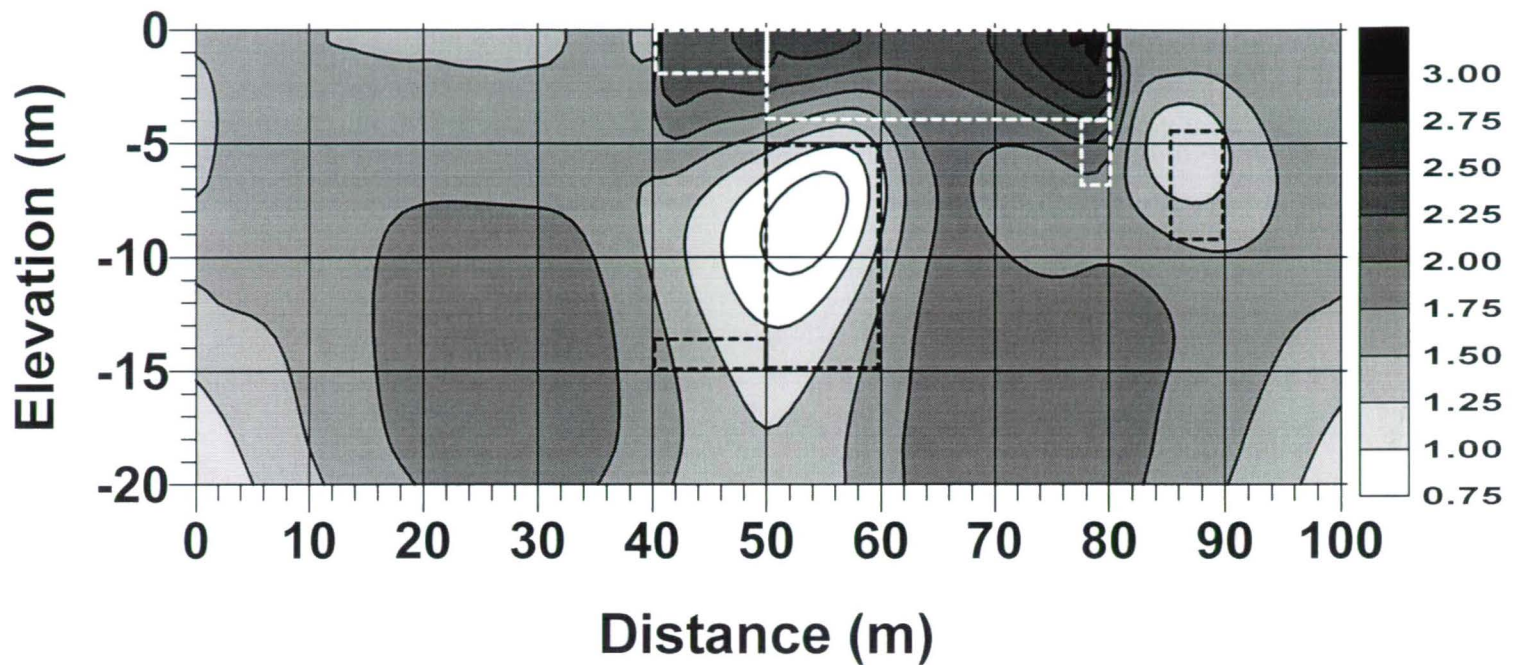


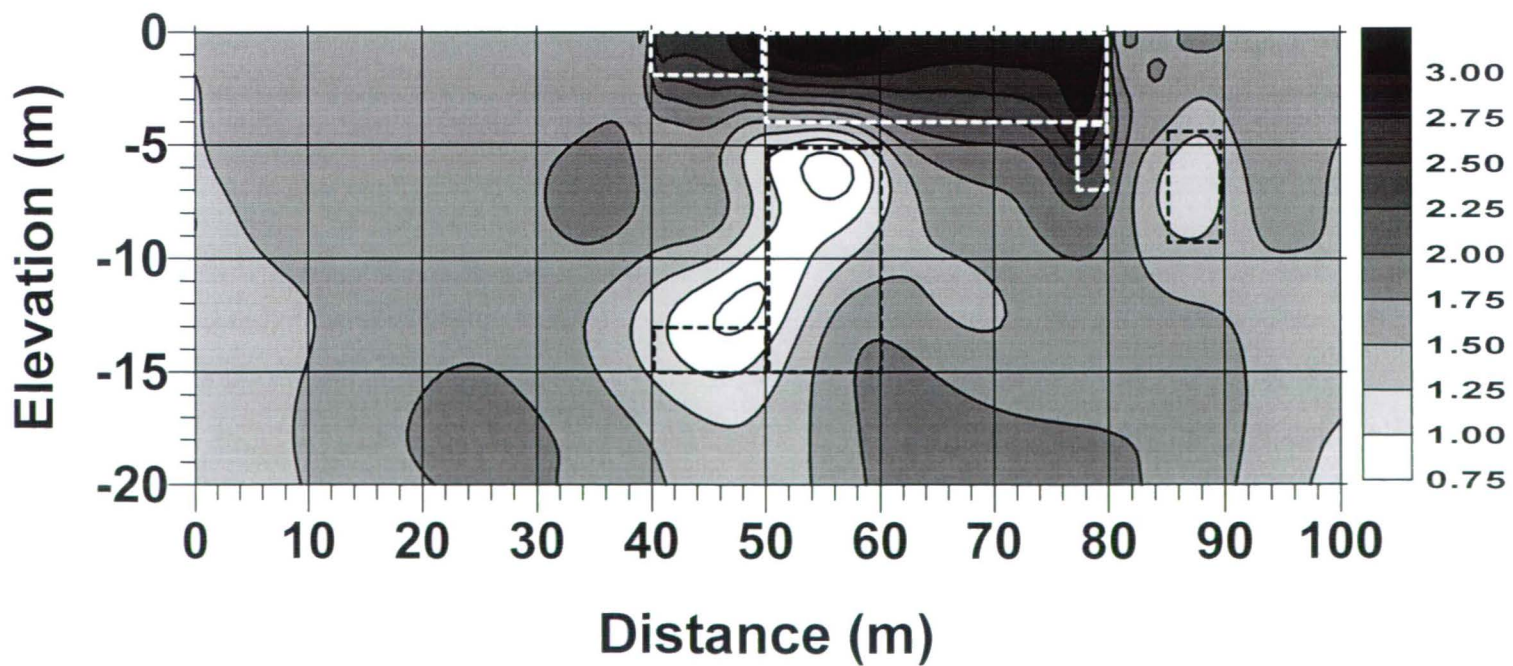
Fig. 4.6

Model 2 TM-mode

a) 1 Frequency



b) 4 Frequencies



Cross-section contoured using the logarithm of resistivity. Scale bar in log (resistivity ohm.m)

Field example 1 TE-mode 16 kHz

Comparison of observed and modelled results

2d NLCG. 2% assigned data errors give rms misfits of 5% (line), 4%(dash)

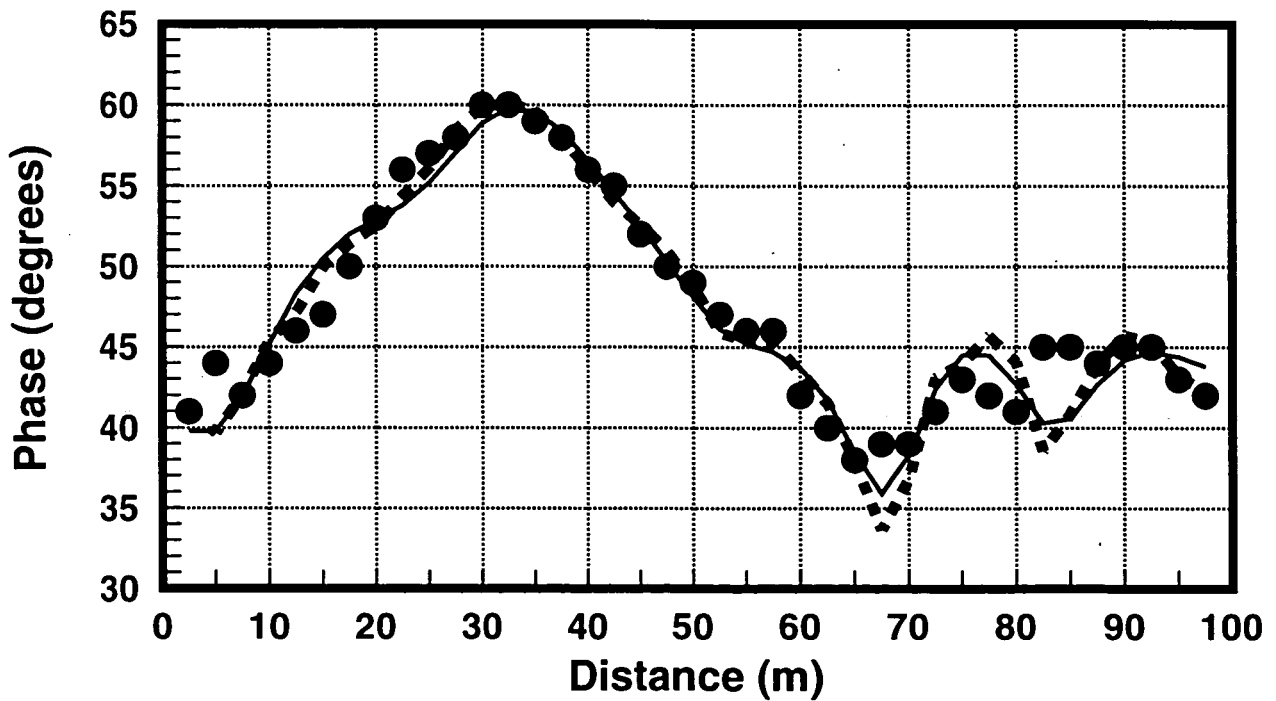
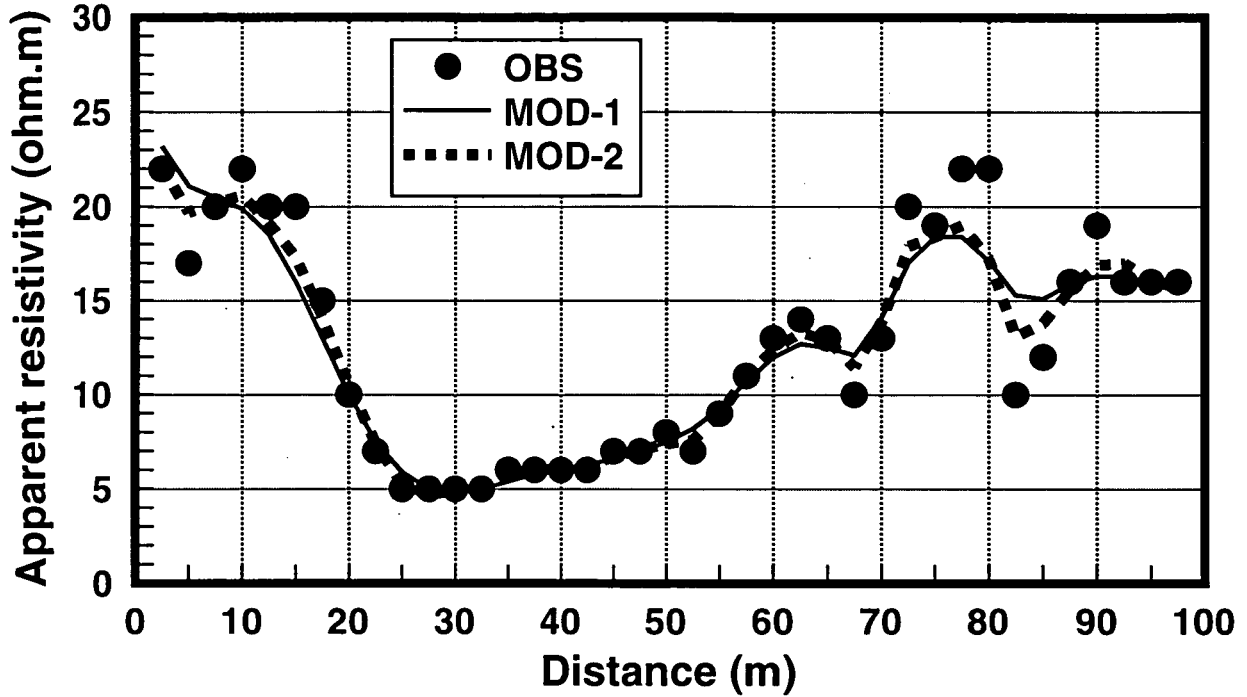
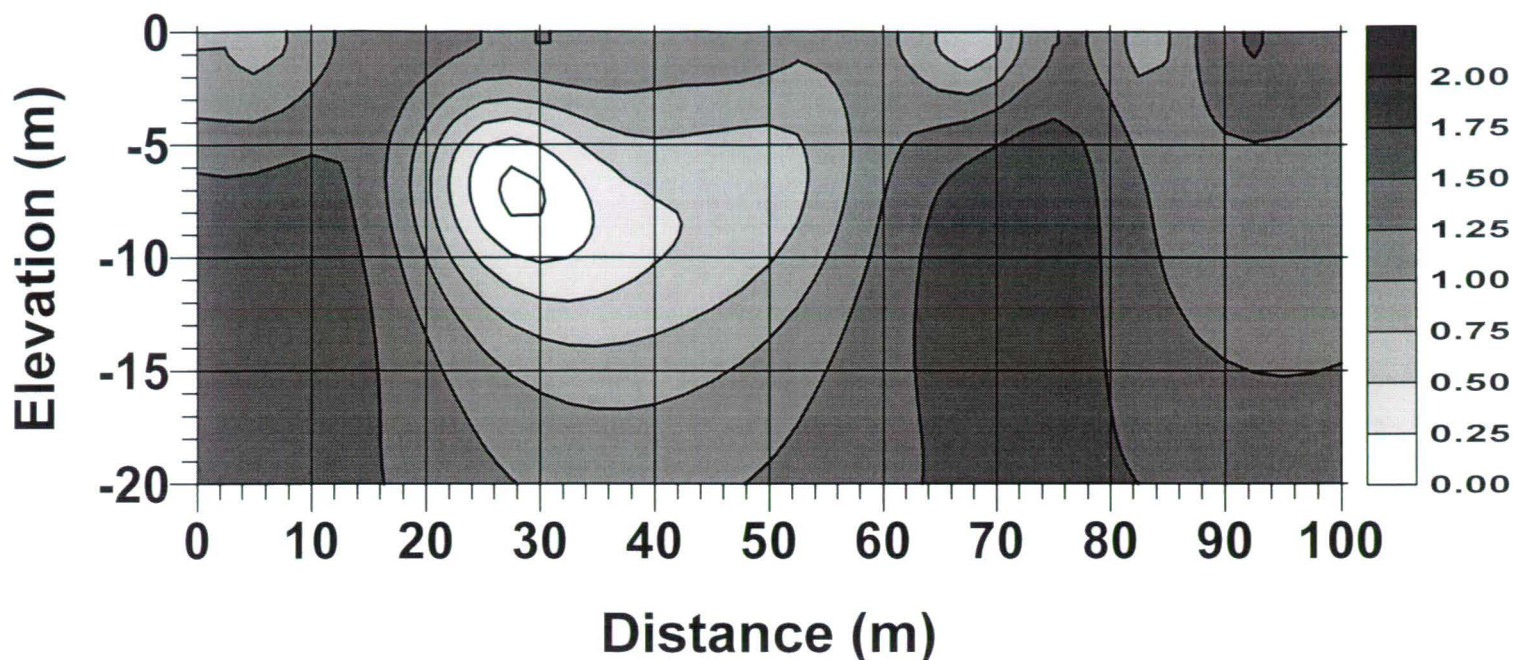


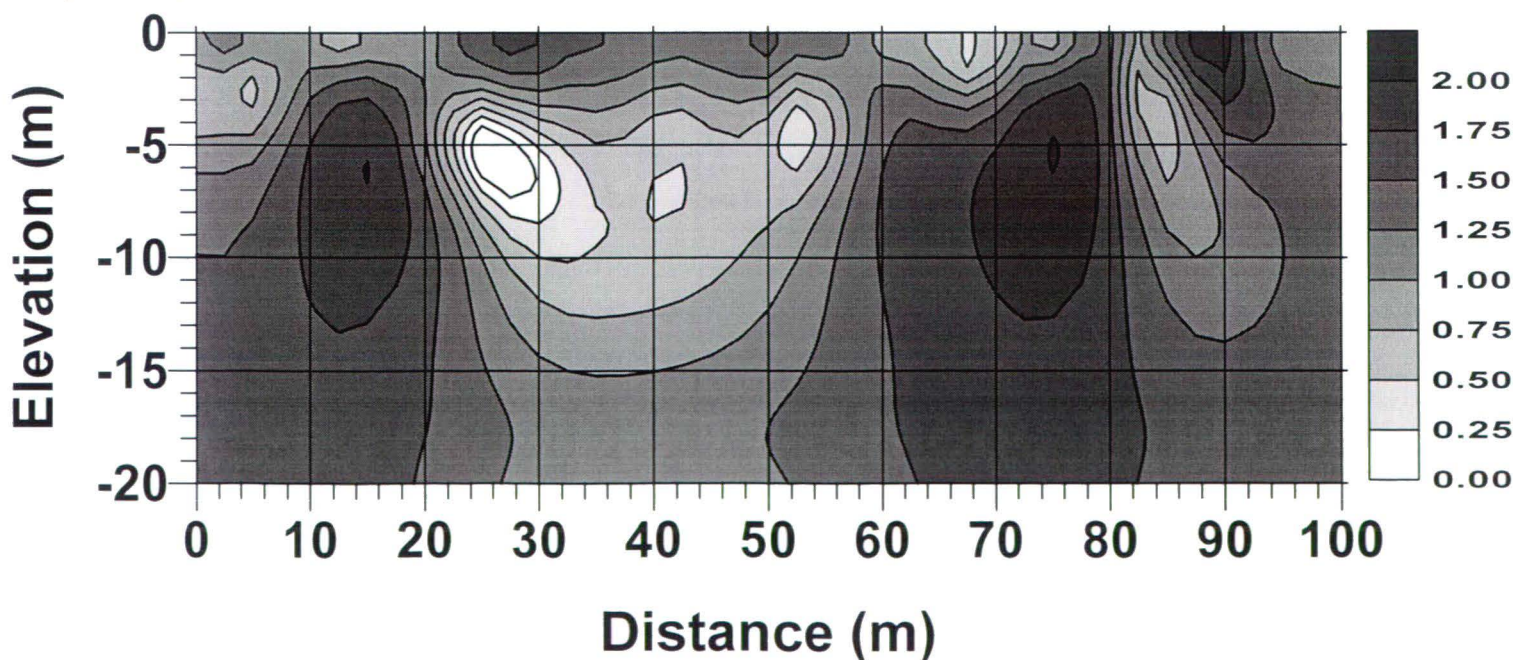
Fig. 5.2

Field example 1 TE-mode 16 kHz

a) $T=30$, rms misfit=5%



b) $T=1$, rms misfit=4%



Cross-section contoured using the logarithm of resistivity. Scale bar in log (resistivity ohm.m)

Field example 2 TM-mode 16 kHz

Comparison of observed and modelled results

2d NLCG. 2% assigned data errors give rms misfits of 5% (line), 3.6%(dash)

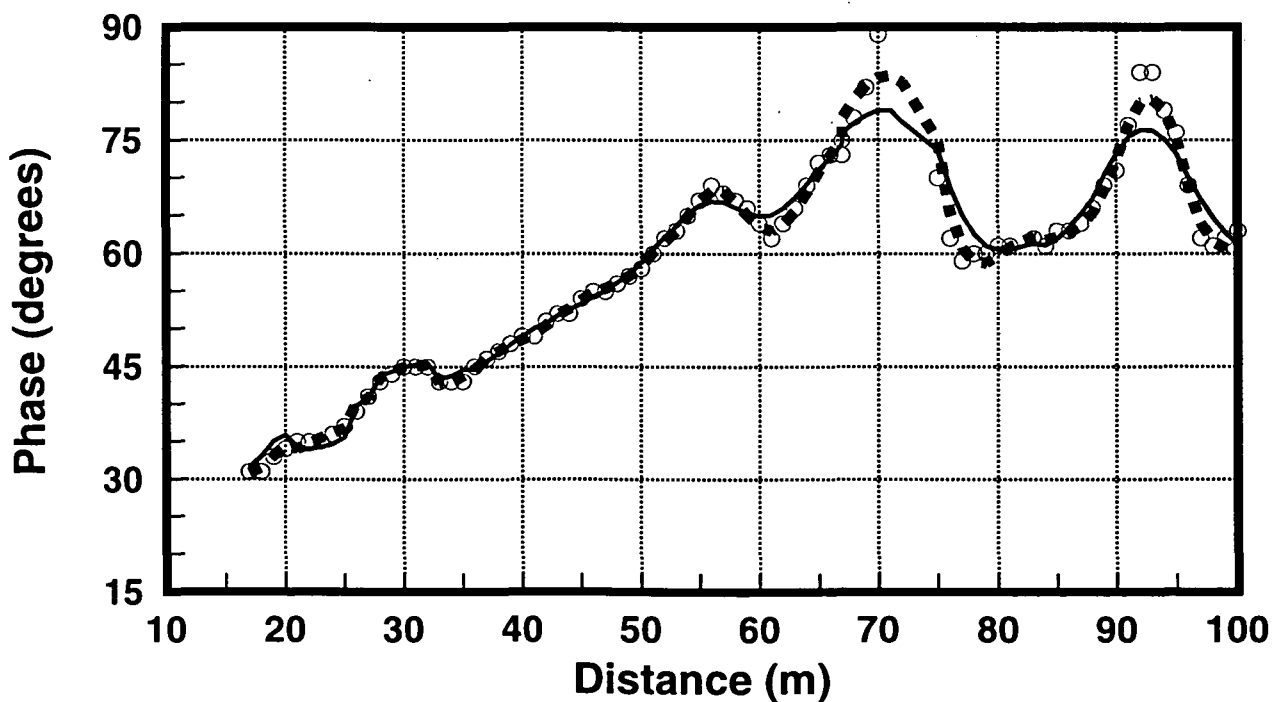
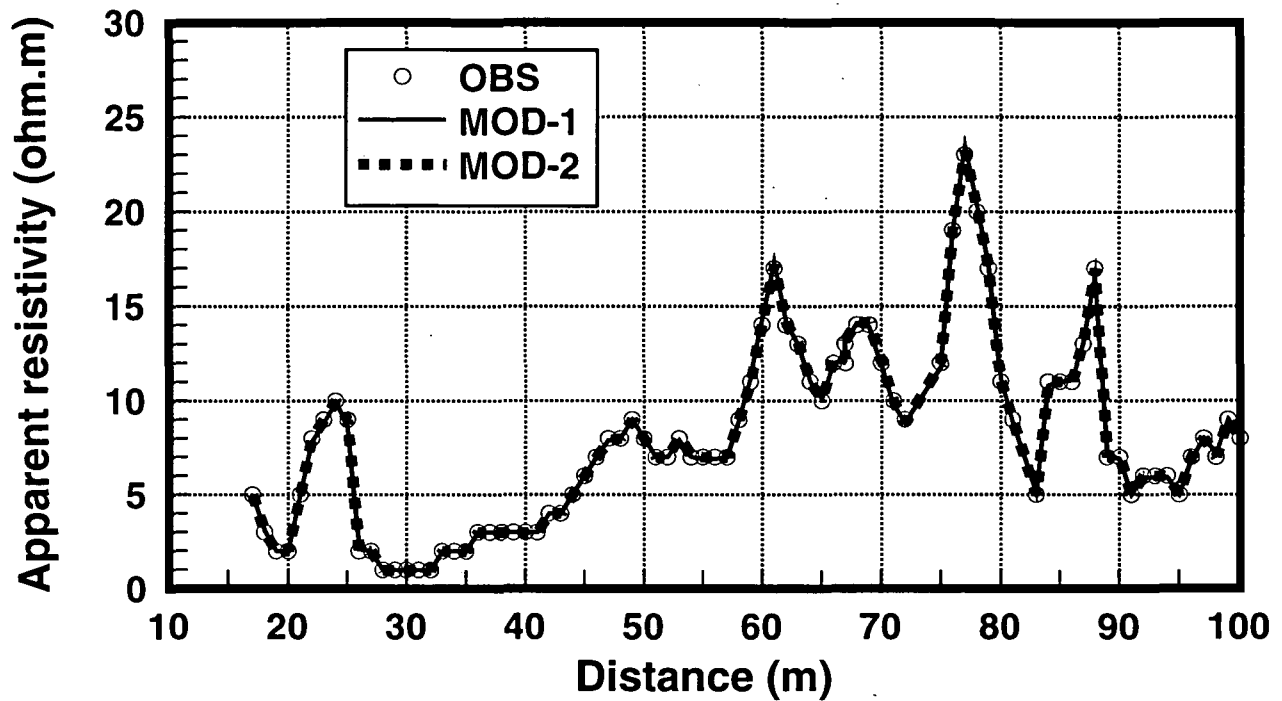
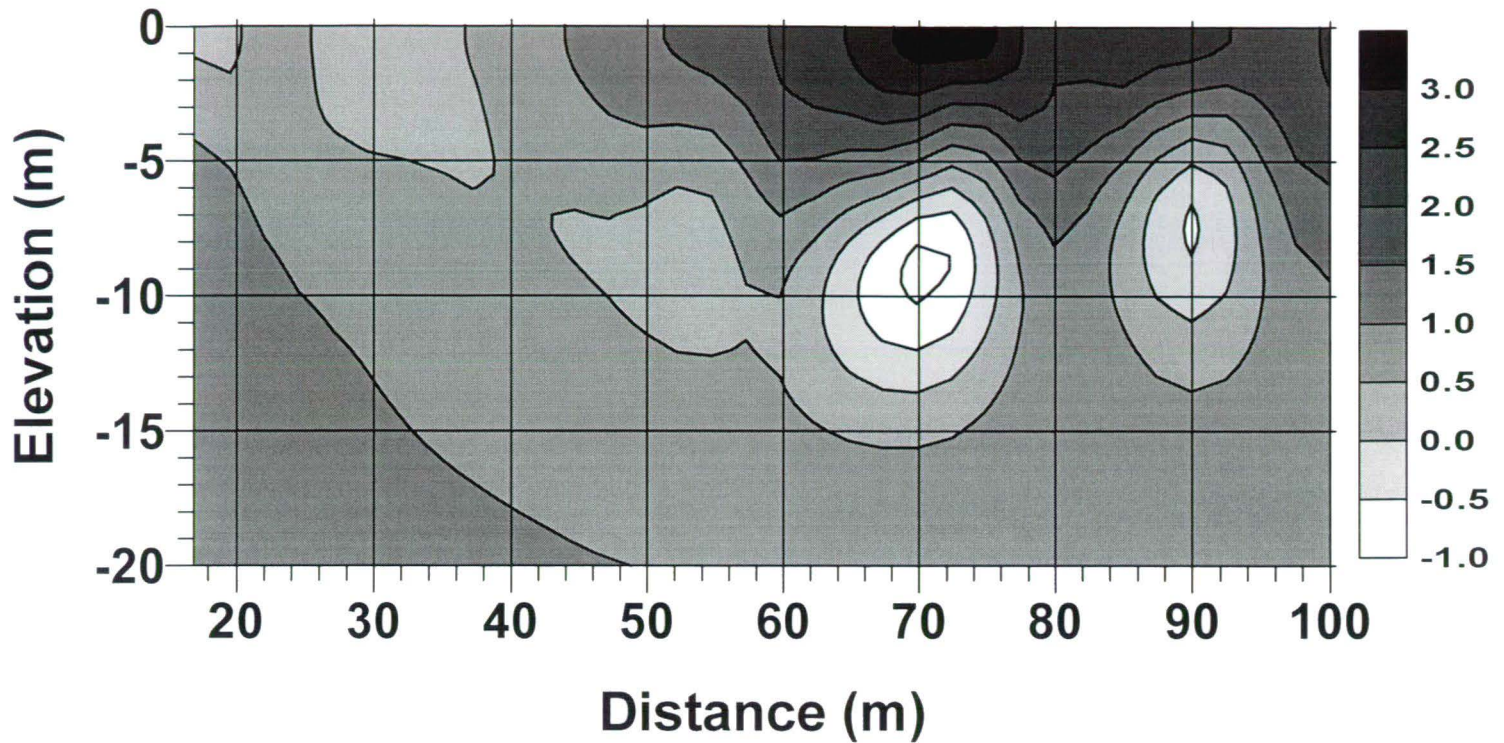


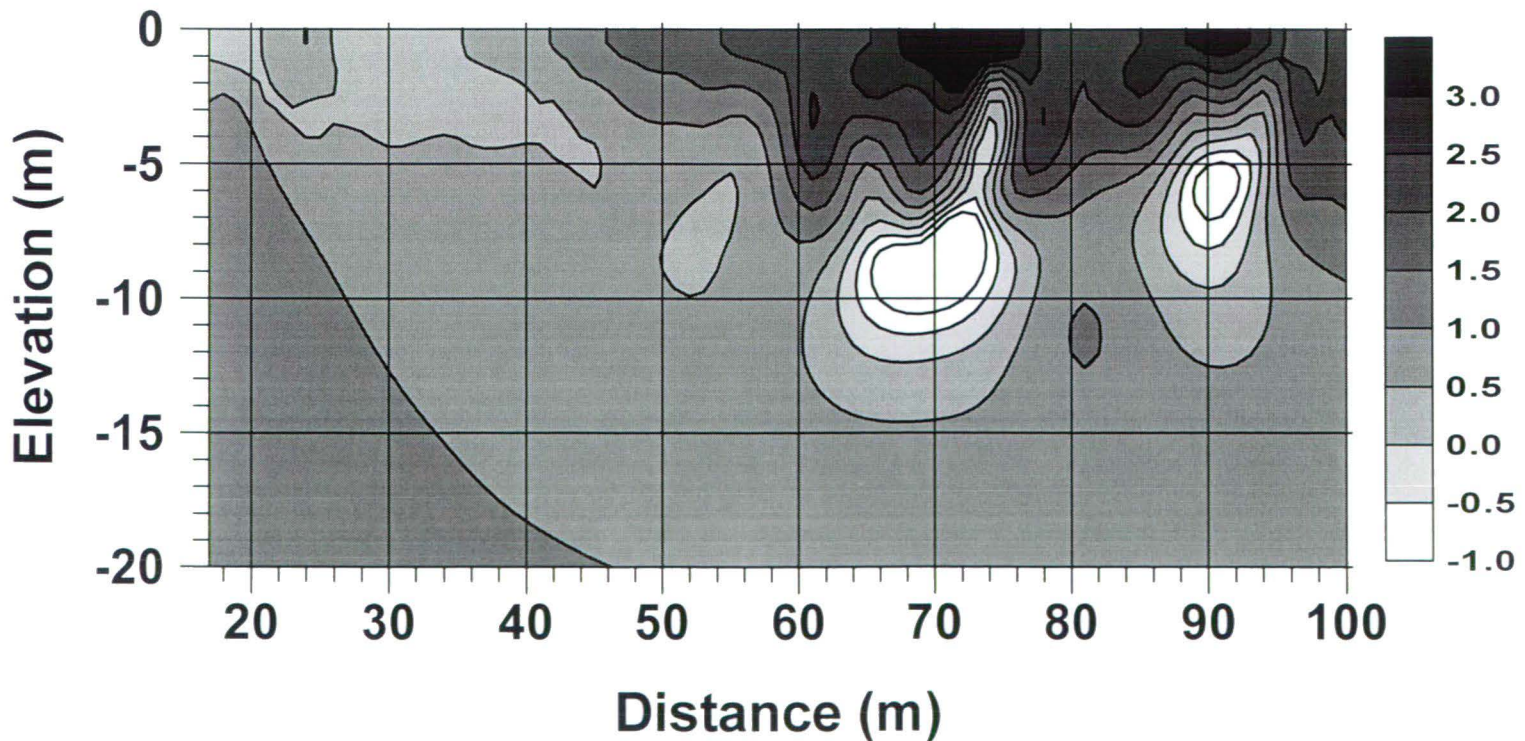
Fig. 5.4

Field example 2 TM-mode 16 kHz

a) $T=30$, rms misfit=5%



b) $T=1$, rms misfit=3.6%



Cross-section contoured using the logarithm of resistivity. Scale bar in log (resistivity ohm.m)